604 *Chem. Mater.* **2010,** *22,* 604–611
DOI:10.1021/cm901591d

CHEMISTRY OF MATERIALS
Review

New bulk Materials for Thermoelectric Power Generation: Clathrates and Complex Antimonides[†]

Holger Kleinke*

Department of Chemistry, University of Waterloo, Waterloo, Ontario, Canada N2L 3G1

Received June 9, 2009. Revised Manuscript Received August 7, 2009

Thermoelectric power generation is foreseen to play a much larger role in the near future, considering the need for alternative energies because of declining natural resources as well as the increasing efficiency of thermoelectric materials. The latter is a consequence of the discoveries of new materials as well as of improvements of established materials by, for example, nanostructuring or band structure engineering. Within this review, two major classes of high-temperature thermoelectrics are presented: clathrates formed by silicides and germanides, and complex antimonides including but not limited to the filled skutterudites. The clathrates and the skutterudites are cage compounds that exhibit low thermal conductivity, reportedly related to the rattling effect of the guest atoms, whereas the other antimonides achieve low thermal conductivity via defects or simply via the high complexity of their crystal structures.

1. Introduction

With the increasing awareness of the declining global energy resources, alternative methods of power generation, e.g., those based on the thermoelectric energy conversion, become increasingly important. Thermoelectric materials are capable of converting heat (more precisely, a temperature gradient, ΔT) into electricity.[1,2] Considering that more than half of all the energy generated by mankind is transformed into waste heat, recovering any part of that waste heat via thermoelectrics would be extremely beneficial.[3] For example, thermoelectrics could recover energy from the waste heat of the exhaust system of automobiles. This electricity production with current state-of-the-art thermoelectrics may lead to fuel economy improvements of about 5% by reducing the alternator load on the engine.[4] In a hybrid containing an electrical engine, the so-gained electricity may be employed to charge its battery, causing additional economy improvements.[5] Finally, advanced thermoelectrics of the near future could generate enough energy from the exhaust heat to replace the alternator. Moreover, thermoelectric generators can be utilized to directly convert solar thermal energy into electricity, at longer wavelengths than—and thus in addition to—the photovoltaics.[6]

Because the thermoelectric energy conversion is a solid state technique without any moving parts, thermoelectrics exhibit extreme reliability and longevity, evident from the successful use of thermoelectrics for power generation in outer-planet spacecrafts (Voyager, Ulysses, Galileo, and Cassini) since the 1970s. Significant increases in the efficiency of the thermoelectric power generation, which still remains below 10% in the devices on the market, are required to enable thermoelectrics to replace environmentally more harmful energy conversion methods on a global scale, and increase the quantity of energy extractable from waste heat. Thermoelectrics are therefore currently used when reliability is of utmost importance, like in subsea or space applications, as well as in the telecommunication industry for power generation in remote locations.[7]

The thermoelectric efficiency depends on the temperatures used (Carnot term) as well as on the thermoelectric figure-of-merit, ZT. This dimensionless figure-of-merit is defined as $ZT = TS^2\sigma/\kappa$, with S = Seebeck coefficient, σ = electrical conductivity, κ = thermal conductivity. Because high ZT values translate into a high power conversion efficiency, η (eq 1), advanced thermoelectrics exhibit high Seebeck coefficient and high electrical conductivity combined with low thermal conductivity.[7,8]

$$\eta = \frac{T_H - T_C}{T_H} \frac{\sqrt{1+ZT}-1}{\sqrt{1+ZT}+T_C/T_H} \quad (1)$$

Unfortunately, these properties cannot be independently optimized, which impedes progress in thermoelectric research. For example, the electrical conductivity is proportional to the charge carrier concentration, while the Seebeck coefficient decreases with increasing charge carrier concentration. The thermal conductivity also increases with the charge carrier concentration. Therefore, metals with a large carrier concentration exhibit an advantageous high electrical conductivity, but a disadvantageous small Seebeck coefficient and high thermal conductivity. On the other hand, insulators cannot be employed because of their obvious lack of electrical conductivity, resulting in ZT values around zero.

[†] Accepted as part of the 2010 "Materials Chemistry of Energy Conversion Special Issue".

*To whom correspondence should be addressed. E-mail: kleinke@uwaterloo.ca.

 Published on Web 08/25/2009

Typical thermoelectrics are therefore neither metals nor insulators, but narrow gap semiconductors with intermediate charge carrier concentrations of the order of 1×10^{19} to 1×10^{21} carriers/cm^3. On the basis of theory, thermoelectrics should comprise band gaps of at least $6\,k_BT$, with k_B = Boltzmann constant and T = temperature, i.e., at least 0.16 eV at 300 K.[9] Such semiconductors may exhibit values on the order of $S = \pm 100\ \mu VK^{-1}$, $\sigma = 1000\ \Omega^{-1}\,cm^{-1}$, $\kappa = 1\ W\,m^{-1}\,K^{-1}$, yielding $ZT = 0.3$ at 300 K.

High complexity of the crystal structure is another important criterion, because this reflects into a large Seebeck coefficient and a small thermal conductivity. The former is a consequence of spikes in the densities of states, DOS, causing a large first derivate of DOS, which in turn is proportional to the Seebeck coefficient via the Mott eq 2, with e = charge of an electron, E = energy, E_F = Fermi energy[10−12]

$$S = \frac{\pi^2 k_B^2}{3e} T \left| \frac{\partial[\ln\sigma(E)}{\partial E} \right|_{E=E_F} ; S \propto \frac{1}{DOS(E_F)} \left| \frac{\partial[DOS(E)]}{\partial E} \right|_{E=E_F} \quad (2)$$

Moreover, the thermal conductivity is composed of the electronic term, κ_e, and the lattice contribution, κ_l: $\kappa = \kappa_e + \kappa_l$. As expressed in the Wiedemann−Franz−Lorenz law, κ_e is proportional to σ:[13] $\kappa_e = LT\sigma$, where L = Lorenz factor.[14] The small thermal conductivity of complex structures is a consequence of the decrease in the mean free path length of the phonons, causing a small κ_l. In addition, the inclusion of nanodomains is known to lower κ_l as well.[15−17] Ideally, the structure would impede only the phonon movement, not the electrons. This concept is known as PGEC: phonon glass, electron crystal;[18,19] PGEC materials behave as a glass with respect to phonon scattering (low thermal conductivity) and as a crystal with respect to electron scattering (high electrical conductivity). Finally, as materials consisting of heavy elements are generally known to have low lattice thermal conductivity, for heavy elements reduce the atomic vibration frequencies most currently known thermoelectrics are based on such heavy elements.

Two relatively new material classes are widely regarded as PGEC, namely the clathrates[20] and the filled skutterudites.[21] These compounds are reviewed in this article along with related complex antimonides[22] for power generation at elevated temperatures. Including all high temperature thermoelectrics, such as oxides,[23,24] tellurides,[15,25−27] and intermetallics (e.g., half Heusler phases),[28,29] would go beyond the scope of this short review.

2. Clathrates

The word "clathrate" is generally used in chemistry to describe a cage structure formed by the host atoms that includes the so-called guest atoms. Earliest examples are ice clathrates (crystalline H_2O) that includes Cl_2 molecules as guest.[30,31] Most clathrates of interest with respect to the thermoelectric energy conversion are formed by elements of the groups 13 and 14 (triels and tetrels) as host atoms, and the cationic guests are group 1 or group 2 cations. Clathrate I type materials are of the general formula A_8E_{46}, with A = Na, K, Ba; E = Al, Ga, In, Si, Ge, Sn, adopting the cubic space group $Pm\bar{3}n$ with the lattice parameter a of the order of 10 Å, depending on the constituent elements.[32] Clathrates II and III have idealized formulas of $A_{24}E_{136}$ and $A_{30}E_{172}$, respectively, and exist with the same A and E elements,[33−36] but examples adopting these structures are very rare, and reports of their thermoelectric properties extremely scarce.

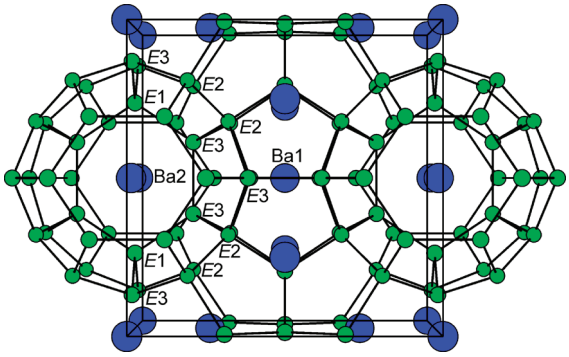

Figure 1. Crystal structure of cubic $Ba_8Ga_{16}Si_{30}$. All three E sites are mixed occupied by Ga and Si.

In the context of the Zintl concept,[37] the electropositive A atoms transfer their valence-electrons to the E atoms in Zintl compounds A_xE_y, which form a three-dimensional anionic framework in the clathrates I. All E atoms are surrounded by four other E atoms, like Si in the diamond structure. The clathrate A_8E_{46} is thus a typical semiconducting Zintl compound, when all E atoms comprise four valence-electrons after complete electron transfer from the A atoms, i.e., in the case of $46 \times 4 = 184$ valence-electrons per formula unit.[38] This is true in the case of $Ba_8Ga_{16}Si_{30}$ and $Sr_8Ga_{16}Ge_{30}$,[39] with Ba/Sr supplying two, Ga three, and Si/Ge four valence-electrons: $8 \times 2 + 16 \times 3 + 30 \times 4 = 184$. Alternatively, assigning oxidation states according to $(Sr^{2+})_8(Ga^{1-})_{16}(Ge^0)_{30}$ implies that both the Ga and the Ge atoms are each provided with four electrons. Nevertheless, the triels (here: Ga) exhibit a clear site preference for the sites $E1$ on 6c and $E3$ on 24k (the sites of the six ring), compared to $E2$ on 16i (the tetrahedral site), while minimizing the less favorable Ga−Ga bonds.[40] The crystal of $Ba_8Ga_{16}Si_{30}$, a clathrate I material with mixed Ga/Si occupancies,[41] is shown in Figure 1.

Two types of cages exist in the clathrate I structure; one is a (pentagonal) dodecahedron, filled with the Ba1 atom on Wyckoff site 2a, and the other is best described as a tetrakaidecahedron with two hexagonal and 12 pentagonal faces, filled with the Ba2 atom (Figure 2). This results in huge coordination numbers of 22 for Ba1 and 24 for Ba2.

Because the tetrakaidecahedron is much larger than the dodecahedron, the $A2$ atoms are not exactly located in its center (6d site), but on four split sites (24j, each with

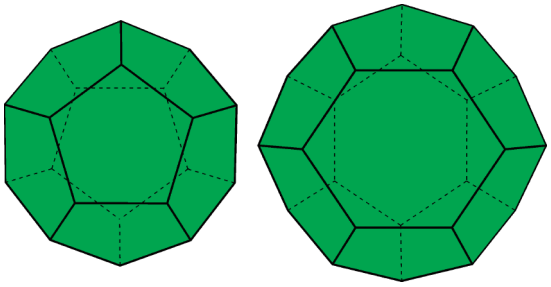

Figure 2. Coordination polyhedra of the Ba atoms of $Ba_8Ga_{16}Si_{30}$. Left, Ba1-centered dodecahedron; right, Ba2-centered tetrakaidecahedron.

25% occupancy) around the center to yield reasonable $A-E$ distances.[42,43] Still, even when refined as split sites, both A cations exhibit enlarged anisotropic displacement parameters, ADPs, and may thus viewed as rattlers. This rattling, i.e., the enhanced vibration, of the guest atoms A causes a flattening of the phonons bands, lowering the velocity of the phonons, which significantly contributes to the low thermal conductivity of these materials.[44] Therefore, clathrates are considered as PGEC materials.[32]

Several band structure calculations revealed narrow-gap semiconducting properties of clathrates I with the ideal number of 184 valence-electrons, including $Sr_8Ga_{16}Ge_{30}$, $Ba_8Ga_{16}Ge_{30}$, $Ba_8Ga_{16}Si_{30}$, $Ba_8In_{16}Sn_{30}$[45] and $Ba_8Al_{16}Ge_{30}$.[46] This is in accord with the electron counting based on the Zintl concept demonstrated above. With calculated band gaps between 0.2 and 0.6 eV, all the basic criteria for enhanced thermoelectrics are met. Both n- and p-type clathrates have been studied, and ZT may possibly exceed one at high temperatures, for example in n-type $Yb_{0.5}Ba_{7.5}Ga_{16}Ge_{30}$ with $ZT = 1.1$ at 950 K (measured on a polycrystalline sample after spark plasma sintering), where two different cations, Yb and Ba, occupy the A sites.[47] It should be noted, however, that the originally reported successful incorporation of Yb into this clathrate may be doubtful.[48,49]

The current record for a clathrate was observed in a single crystal of $Ba_8Ga_{16}Ge_{30}$ with $ZT = 1.35$ at 900 K, extrapolated to reach 1.63 at 1100 K.[50] High ZT values of n-type clathrates in bulk form were measured to be 0.72 in the case of $Sr_8Ga_{15.5}In_{0.5}Ge_{30}$ at 800 K,[51] and estimated to be 0.7 in the case of $Ba_8Ga_{16}Ge_{30}$ at 700 K and 0.87 in the case of $Ba_8Ga_{16}Si_{30}$ at 870 K,[52] values that compare well with $ZT = 0.61$ for p-type $Ba_8Ga_{16}Al_3Ge_{27}$ at 760 K.[53] An overview of these ZT values, along with other high-temperature thermoelectrics, is presented in Table 1.

These clathrates with high ZT values can exhibit quite different values for the Seebeck coefficient, for example around $S = -60\ \mu V\ K^{-1}$ in case of $Yb_{0.5}Ba_{7.5}Ga_{16}Ge_{30}$ and $S = -80\ \mu V\ K^{-1}$ in case of $Sr_8Ga_{15.5}In_{0.5}Ge_{30}$ and $S = +190\ \mu V\ K^{-1}$ in case of $Ba_8Ga_{16}Al_3Ge_{27}$ at room temperature. The electrical conductivity is typically of the order of $10^{+3}\ \Omega^{-1}\ cm^{-1}$, whereas the thermal conductivity is below 2 W $m^{-1}\ K^{-1}$. Considering the many possible variations of these clathrates together with the fact that many such investigations have just begun, even higher ZT values are likely to be found during the next few years.

Table 1. ZT_{max} Values of Selected High-Temperature Thermoelectrics[a]

compd (type)	ZT_{max}	T_{max} (K)
$Ba_8Ga_{16}Al_3Ge_{27}$ (p)[53]	0.61	763
$Yb_{0.5}Ba_{7.5}Ga_{16}Ge_{30}$ (n)[47]	1.09	950
$Ba_8Ga_{16}Ge_{30}$ (n)[50]	1.35	900
$Ba_8Ga_{16}Si_{30}$ (n)[52]	(0.87)	873
$Ba_8Ga_{16}Ge_{30}$ (n)[52]	(0.70)	700
$Ba_{0.13}In_{0.14}Co_4Sb_{11.75}$ (n)[65]	1.19	850
$LaFe_3CoSb_{12}$ (p)[72]	(1.40)	1000
$Ba_{0.24}Co_4Sb_{12}$ (n)[79]	1.10	850
$Ca_{0.18}Co_{3.97}Ni_{0.03}Sb_{12.4}$ (n)[78]	0.99*	800
$Yb_{0.19}Co_4Sb_{12}$ (n)[77]	1.14*	638
β-Zn_4Sb_3 (p)[54]	1.30	673
$YbZn_{0.4}Cd_{1.6}Sb_2$ (p)[62]	1.20*	700
$Yb_{14}MnSb_{11}$ (p)[55]	1.04	1228
$Mo_3Sb_{5.4}Te_{1.6}$ (p)[57]	0.76*	1050
$Ni_{0.06}Mo_3Sb_{5.4}Te_{1.6}$ (p)[112]	0.93*	1023

[a] Values in parentheses are postulated. Values with an asterisk indicate that the measurement was stopped before reaching a maximum, either because of the experimental setup or the decomposition of the material.

3. Complex Antimonides

3.1. Filled Skutterudites. The largest class of thermoelectric antimonides is formed by the skutterudites.[21] These materials are being considered for use in automobiles for energy recovery from the exhaust heat.[5] Other Sb-based high-temperature thermoelectrics are β-Zn_4Sb_3,[54] $Yb_{14}MnSb_{11}$,[55] and $A_yMo_3Sb_{7-x}Te_x$,[56−59] all with maximal ZT values around 1.0. Moreover, materials based on AZn_2Sb_2 in the $CaAl_2Si_2$ type can achieve ZT values >0.5 as well, e.g., $CaZn_2Sb_2$ 0.56 at 773 K,[60] $YbZn_{1.9}Mn_{0.1}Sb_2$ 0.65 at 736 K,[61] and $YbZn_{0.4}Cd_{1.6}Sb_2$ even 1.2 at 700 K.[62]

The word "skutterudite" stems from the Skutterud, a town in Norway, where $CoAs_3$—the skutterudite aristotype—was found. Many variants MQ_3 exist with M = late transition metal, Q = P, As, Sb. Like the clathrate I, the skutterudite crystallizes in a cubic space group, namely in $Im\bar{3}$, a distorted variant of the ReO_3 type. In contrast to ReO_3, the corner-sharing MQ_3 octahedra are tilted in the skutterudite structure, so that planar Q_4 rectangles with $Q-Q$ bonds occur as well as large empty Q_{12} icosahedra. The latter may be filled with alkaline or rare earth metals, leading to the filled skutterudites of the general formula $Ln_xM_4Q_{12}$ (with $x \leq 1$), with $LaFe_4Sb_{12}$ being the first antimonide[63] (Figure 3).

Because the icosahedral cage is somewhat large for the Ln atoms, the corresponding $Ln-Sb$ interactions are long, e.g. 3.41 Å in $LaFe_4Sb_{12}$. Therefore, the Ln ADPs are typically much larger than the other APDs, e.g., by a factor of 5−6 in case of $LaFe_4Sb_{12}$[63] and 3−4 in case of $LaFe_3CoSb_{12}$.[64] This observation is generally interpreted as the rattling effect, causing a decrease in lattice thermal conductivity upon adding the filler atoms. Double-filled skutterudites[65] may exhibit even better thermoelectric properties.

Although evidence for the decrease in lattice thermal conductivity is abundant, e.g., at least 1 order of magnitude for filled variants of $IrSb_3$,[66] recent inelastic neutron scattering experiments on $LaFe_4Sb_{12}$ and $CeFe_4Sb_{12}$ revealed evidence for significant host−guest coupling; the authors concluded that the filled skutterudite is better

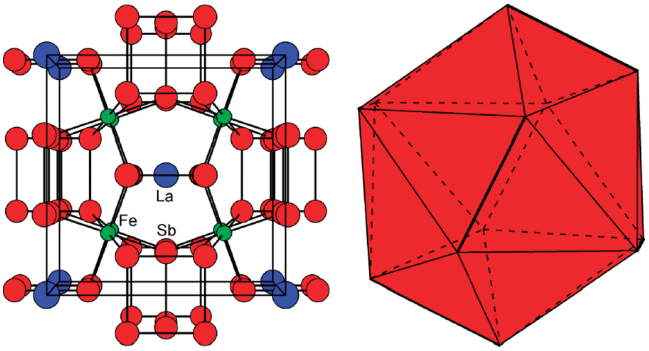

Figure 3. Crystal structure of cubic $LaFe_4Sb_{12}$ (left) and the coordination polyhedron of the La atom, the $LaSb_{12}$ icosahedron (right).

described as "an electron crystal and a phonon crystal", not as a PGEC material.[67]

The $Q-Q$ distances of the planar rectangles are comparable to single bonds, albeit slightly elongated. For example, the Sb−Sb distances are 2.90 and 2.98 Å in $CoSb_3$, and 2.80 Å and 2.92 Å in $RhSb_3$,[68] with Sb−Sb single bonds being of the order of 2.8−2.9 Å.[69−71] As demonstrated for the clathrates, the skutterudites can be treated as (transition metal) Zintl compounds: the Q atoms comprise six valence-electrons after being reduced by the M (and Ln) atoms, and achieve the octet via two $Q-Q$ single bonds per Q atom, resulting in Sb_4^{4-} units in $CoSb_3$ and $RhSb_3$. A difference to the clathrates is that the transition metal, such as Co, retains some of its valence-electrons in its d orbitals. The filled skutterudites LnM_4Q_{12} are electron precise semiconductors when six d electrons are located in the nonbonding t_{2g}-like states of the M atoms, yielding $4 \times 6 + 12 \times 6 = 96$ valence-electrons per formula unit. This number is reached in case of $LaFe_3CoSb_{12}$ with $1 \times 3 + 3 \times 8 + 1 \times 9 + 12 \times 5 = 96$, which was extrapolated to reach $ZT = 1.4$ at 1000 K.[72]

Numerous band structure calculations on filled skutterudites[66,73−76] have confirmed the existence of a narrow band gap of the order of 0.5 eV at 96 valence-electrons per formula unit, one example being p-type $LaFe_3CoSb_{12}$. Several n-type filled skutterudites exhibit great thermoelectric performances as well, e.g., $Yb_{0.19}Co_4Sb_{12}$ with ZT(640 K) = 1.14,[77] $Ca_{0.18}Co_{3.97}Ni_{0.03}Sb_{12.4}$ with ZT(800 K) = 0.99,[78] $Ba_{0.13}In_{0.14}Co_4Sb_{11.75}$ with ZT(850 K) = 1.19,[65] $Ba_{0.24}Co_4Sb_{12}$ with ZT(850 K) = 1.10.[79] Therefore, both the bottom of the conduction band and the top of the valence band are of vital importance. Flat bands occur in these areas, indicative of high effective masses, and thus a large Seebeck coefficient. Room temperature Seebeck values of the best filled skutterudites are typically around ± 100 $\mu V\ K^{-1}$, electrical conductivity between 650 $\Omega^{-1}\ cm^{-1}$ and 3200 $\Omega^{-1}\ cm^{-1}$, whereas the thermal conductivity may vary between 3 $W\ m^{-1}\ K^{-1}$ and 5.5 $W\ m^{-1}\ K^{-1}$. It is noted that the clathrates generally possess lower electrical and lower thermal conductivity, while the ZT values may be comparable. Thus far the best filled skutterudites are all Co-based antimonides, i.e., variants of $CoSb_3$, with mostly lanthanide or alkaline earth metals (e.g., Ba) as filler atoms, whereas the best clathrates are typically based on Ba germanides.

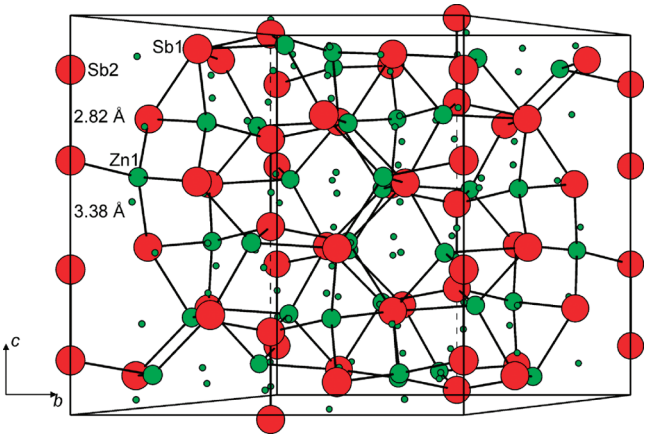

Figure 4. Crystal structure of rhombohedral β-Zn_4Sb_3. The distances refer to the linear Sb atom chain. Small green circles indicate the Zn positions with < 10% occupancy.

3.2. β-Zn_4Sb_3. In contrast to the large families of the skutterudites and the clathrates, only very few variants of β-Zn_4Sb_3[54] are known to exhibit good thermoelectric properties. Hot-pressed β-Zn_4Sb_3 attains ZT = 1.3 at 650−670 K.[54,80] This material crystallizes in the rhombohedral space group $R\bar{3}c$, and its structure is composed of $ZnSb_4$ tetrahedra and a linear chain of Sb2 atoms with alternating distances of 2.82 and 3.38 Å. According to a crystal structure study from the year 2004, several sites exhibit only small Zn occupancy factors between 5 and 6% (small circles in Figure 4), whereas the major Zn site, Zn1, is with 90% occupancy also deficient.[81] The so refined formula is $Zn_{3.83}Sb_3$, i.e., slightly Zn-deficient in comparison to the generally used formula Zn_4Sb_3. Another study from the year 2006 confirmed these findings, with a refined, unusually Zn-poor, formula of $Zn_{3.55}Sb_3$ and a microprobe analysis result of $Zn_{3.90}Sb_3$.[82] In 2007, a refinement of the better characterized α-Zn_4Sb_3 resulted in a comparable Zn deficiency, the refined formula being $Zn_{3.81}Sb_3$.[83]

Applying the Zintl concept, the Sb1 atoms are treated as Sb^{3-}, and the Sb2 atoms as part of the Sb_2^{4-} pairs. Ignoring the sites Zn2−Zn4, the crystallographic formula is $(Zn1)_6(Sb1)_3(Sb2)_2$. Considering the $3 \times 3 + 2 \times 2 = 13$ negative charges of the Sb atoms and the normal 2+ valence state for Zn, a "Zn_6Sb_5" is electron deficient; charge balance would be achieved for a "$(Zn^{2+})_{6.5}(Sb1^{3-})_3(Sb2)_2^{4-}$" ($Zn_{13}Sb_{10}$), which corresponds to "$Zn_{3.9}Sb_3$". Electronic structure calculations revealed the existence of a gap of 0.3−0.4 eV at that composition.[76,84] Thus, the above-mentioned refined formulas between $Zn_{3.55}Sb_3$ and $Zn_{3.83}Sb_3$ are all Zn-deficient, which explains the p-type conduction of β-Zn_4Sb_3.

Similar to the clathrates, the best feature of β-Zn_4Sb_3 with respect to thermoelectricity is its low thermal conductivity, determined to be 0.9−1.1 $W\ m^{-1}\ K^{-1}$ at room temperature.[54,80] The Seebeck coefficient is inconspicuous, with room temperature values around +110 $\mu V\ K^{-1}$, and increases linearly with increasing temperature. The electrical conductivity, on the other hand, is 320 $\Omega^{-1}\ cm^{-1}$ at room temperature, rather low, and decreases in

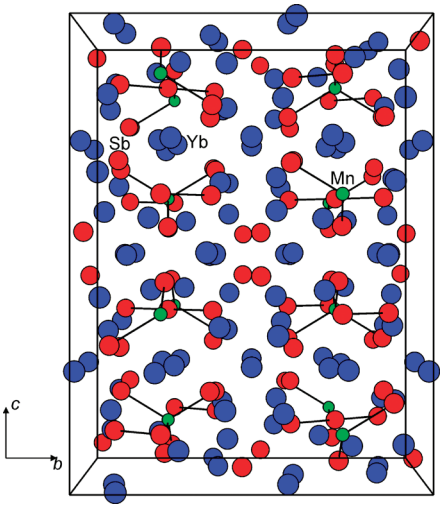

Figure 5. Crystal structure of tetragonal $Yb_{14}MnSb_{11}$.

contrast to the Seebeck coefficient with increasing temperature.

The extraordinarily low thermal conductivity of β-Zn_4Sb_3 is likely a consequence of its complex structure and the highly disordered Zn sites,[81,82] in conjunction with the occurrence of nanodomains.[85] The so-called "dumbbell rattling" of the Sb_2 pairs of the linear chains was determined via inelastic neutron scattering to be an important factor as well, which expresses itself in a large vibration along the chain direction.[86] Band structure calculations also showed that the longer interpair Sb2−Sb2 interaction of 3.38 Å is significant,[76] which may be a driving force for the enlarged vibration in that direction.

β-Zn_4Sb_3 is far from being optimized, however, doping experiments have thus far failed to yield ZT values above 1.3.[87,88] Unfortunately, its phase transition into γ-Zn_4Sb_3 around 670 K limits its useful temperature range, and its brittle character may be problematic as well.[89]

3.3. $Yb_{14}MnSb_{11}$. Another exciting antimonide is $Yb_{14}MnSb_{11}$, which attains after hot-pressing $ZT = 1.1$ at 1275 K,[55] and is therefore being tested at NASA for use in spacecrafts.[8] $Yb_{14}MnSb_{11}$ crystallizes in the $Ca_{14}AlSb_{11}$ type, space group $I4_1/acd$,[90] and contains $MnSb_4$ tetrahedra and linear Sb_3 units with intermediate Sb−Sb bonds of 3.20 Å (Figure 5). This Sb_3 unit is topologically equivalent with the linear I_3^- units of, e.g., CsI_3[91] and $[Ph_4As]I_3$,[92] and linear Se_3^{4-} of $Ba_2Ag_4Se_5$.[93] Therefore, it is most likely isoelectronic, hence comprises 22 valence electrons like in Sb_3^{7-}. Then, the valence-electrons of $Yb_{14}MnSb_{11}$ could readily be assigned in the Zintl tradition according to "$(Yb^{2+})_{14}Mn^{3+}Sb_3^{7-}(Sb^{3-})_8$". Band structure calculations performed on the isovalent main group variants $Ca_{14}AlAs_{11}$[94] and $Ca_{14}AlSb_{11}$[76] confirmed that this assignment of valence electrons may be appropriate, revealing a band gap of 0.7 eV in case of the antimonide. On the other hand, detailed experimental[95] and theoretical investigations (on $Ca_{14}MnBi_{11}$)[96] revealed the presence of a hole, h^+, in the Sb 5p band along with (high spin) Mn^{2+}.

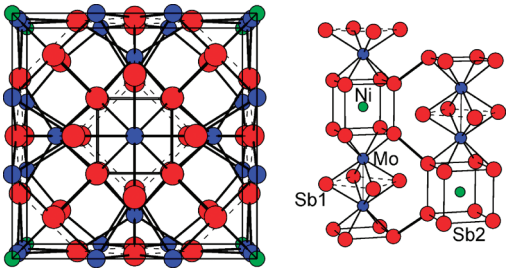

Figure 6. Crystal structure of cubic $Ni_yMo_3Sb_7$ (left) and a fragment of its unit cell (right).

The central atom of the hypervalent Q_3^{7-} unit (Q = P, As, Sb) is often positionally disordered, e.g., in $Ba_{14}InP_{11}$,[97] $Sr_{14}ZnSb_{11}$[98] and $Ba_{14}MnSb_{11}$,[99] and/or exhibits enlarged ADPs, e.g., in $Ca_{14}GaAs_{11}$[100] and $Ca_{14}AlSb_{11}$,[90] in particular toward the terminal Q atoms. The driving force for this distortion is apparently the (dynamic) formation of one shorter Q−Q bond instead of two intermediate ones. This scenario is reminiscent of the "dumbbell rattling" in β-Zn_4Sb_3; however, the ADPs of $Yb_{14}MnSb_{11}$ were reported to be inconspicuous.[101]

Nevertheless, $Yb_{14}MnSb_{11}$ is another example of a material with a very low thermal conductivity, most likely caused by the complexity and relatively high ionicity of its crystal structure (and its heavy constituent elements). Its value decreases from 0.9 W m^{-1} K^{-1} at 300 K to 0.7 W m^{-1} K^{-1} at 1275 K, similar to the situation in β-Zn_4Sb_3. In accord with the hole in the Sb 5p band, a basically temperature-independent carrier concentration of 1×10^{21} holes/cm^3 was observed. Because of the decreasing mobility, the electrical conductivity decreases from 450 Ω^{-1} cm^{-1} at 300 K to 185 Ω^{-1}c m^{-1} at 1200 K, whereas the Seebeck coefficient increases in that temperature range from approximately +60 μV K^{-1} to +185 μV K^{-1}. As a consequence of the rather small values of S and σ at 300 K, ZT(300 K) is below 0.1, but ZT increases steadily to surpass 1.0 around 1150 K.

It may be anticipated that substitution experiments will increase the thermoelectric performance of this material in the near future, because its optimization is still in its beginnings. Improvements on the order of 10% were obtained both with partial substitution of Yb ($Yb_{13.6}La_{0.4}MnSb_{11}$[102]) and of Mn ($Yb_{14}Mn_{1-x}Zn_xSb_{11}$[103] and $Yb_{14}Mn_{1-x}Al_xSb_{11}$[104,105]).

3.4. Mo_3Sb_7. A fourth transition metal containing antimonide of interest is Mo_3Sb_7, which crystallizes in the structure type of Ir_3Ge_7, space group $Im\bar{3}m$.[106] Its structure is comprised of pairs of face-sharing $MoSb_8$ square antiprisms, with an Mo−Mo interaction of 3.00 Å across the Sb_4 square (formed by the Sb1 atoms) with Sb−Sb distances of 3.38 Å. Empty Sb_8 cubes, formed by Sb2 atoms with interatomic distances along the edges of the cube of 3.10 Å, connect the pairs of square antiprisms to linear chains. Three orthogonal chains interpenetrate at the empty $Sb2_8$ cube, and parallel running chains are connected via shorter Sb−Sb bonds of 2.91 Å (bold lines in Figure 6).[56] Small metal atoms can be added to partly fill the $Sb2_8$ cubes, at least up to 14%.[107]

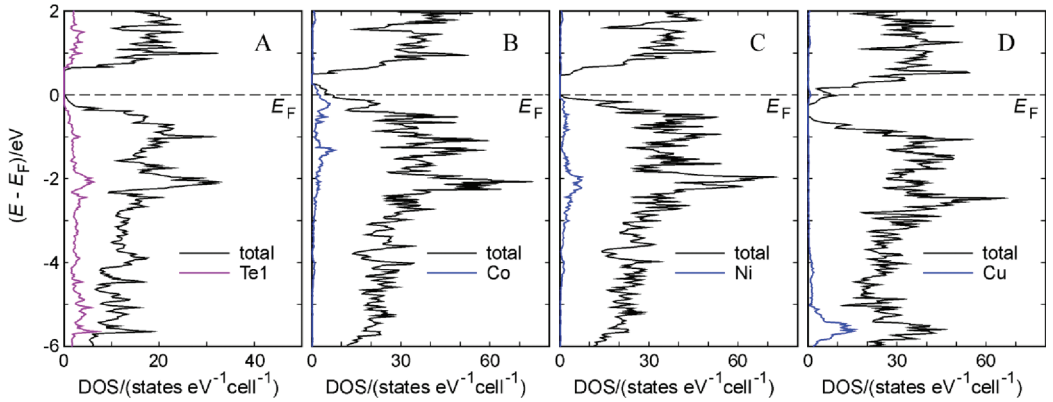

Figure 7. (A) Densities of states of $Mo_3Sb_5Te_2$, (B) $Co_{0.25}Mo_3Sb_5Te_2$, (C) $Ni_{0.25}Mo_3Sb_5Te_2$, and (D) $Cu_{0.25}Mo_3Sb_5Te_2$.

Applying the Zintl concept is impeded by the metallic properties of Mo_3Sb_7 as well as the fractional character of the Sb−Sb bonds. Treating the shortest homonuclear bonds as single bonds, while disregarding the longer interactions, leads to a tentative assignment of Mo^{5+} (with one *d* electron remaining for the Mo−Mo bond), $Sb1^{3-}$ (no Sb−Sb bonds) and $Sb2^{2-}$ (one Sb−Sb bond, hence an $Sb2^{4-}$ pair), thus $(Mo^{5+})_3(Sb1^{3-})_3(Sb2^{2-})_4(h^+)_2$ with h = hole. Despite the metallic character, this electron counting proves itself useful by implying the possibility of semiconducting character after addition of two valence-electrons per formula unit. Indeed electronic structure calculations suggested semiconducting properties for $Mo_3Sb_5Te_2$ with a narrow gap of 0.5 eV.[56] As argued on the basis of electronegativity differences,[56,108] and supported by neutron diffraction experiments,[109] the Te atoms prefer the Sb1 site, because Sb1 participates in the weaker Sb−Sb interactions, compared to Sb2.

Electronic structure calculations also showed that adding cobalt into the cubic voids decreases and adding copper increases the valence-electron concentration, whereas adding nickel does not alter the location of the Fermi level, E_F (Figure 7).[107] The Ni containing antimonide-telluride may thus be understood as $(Ni^{\pm 0})_y(Mo^{5+})_3Sb1^{3-}(Sb2^{2-})_4(Te^{2-})_2$ (with $y \leq 0.5$), i.e., it is semiconducting independent of the Ni concentration. Nevertheless, the Ni content has an impact onto the electronic structures, because the size of the band gap decreases upon Ni addition and the Ni d states increase the number of states below E_F, which is important for the thermoelectric properties of p-type $Ni_yMo_3Sb_{7-x}Te_x$.

Likely due to the metallic character of Mo_3Sb_7, research into its thermoelectric properties just commenced this decade, although Mo_3Sb_7 was reported some 40 years ago.[106] The first report on its thermoelectric properties stems from the year 2002, wherein the Seebeck coefficient was reported to increase with increasing Te content in $Mo_3Sb_{7-x}Te_x$.[56] Complete thermoelectric properties of metallic Mo_3Sb_7 were published for the first time in the year 2009.[110]

Small metal atoms such as *A* = Mg, Fe, Ni, Cu, etc., were added into the cubes formed by the Sb2 atoms, attempting to create the rattling effect and thereby to lower the thermal conductivity.[107] However, the observed increase of the unit-cell dimensions upon intercalation indicates strong interactions between the *A* and the Sb2 atoms (*A*−Sb2 distance: 2.69 Å), which inhibits the rattling effect. Subsequent property measurements actually revealed a slight increase in the thermal conductivity by going from $Mo_3Sb_{5.4}Te_{1.6}$ to $Ni_{0.06}Mo_3Sb_{5.4}Te_{1.6}$.[111]

In comparison to the above-mentioned antimonides β-Zn_4Sb_3 and $Yb_{14}MnSb_{11}$, p-type $Mo_3Sb_{5.4}Te_{1.6}$ exhibits a large electrical conductivity, $\sigma(300\ K) = 1600\ \Omega^{-1}\ cm^{-1}$ or $\sigma(300\ K) = 1700\ \Omega^{-1}\ cm^{-1}$, and a rather high thermal conductivity $\kappa(300\ K) \approx 4.5\ W\ m^{-1}\ K^{-1}$, whereas the Seebeck coefficient, $S = +55\ \mu V\ K^{-1}$, is comparable to that of $Yb_{14}MnSb_{11}$, according to two independent investigations on hot-pressed samples.[57,59] Both the electrical and the thermal conductivity compare well with those of several filled skutterudites.

Adding Ni atoms into the cubic voids of $Mo_3Sb_{5.4}Te_{1.6}$ occurs at room temperature with an increase in *S* to $+68\ \mu VK^{-1}$, in σ to $1800\ \Omega^{-1}\ cm^{-1}$, and in κ to $5.0\ W\ m^{-1}\ K^{-1}$.[59] Hall measurements showed that the increase of the electrical conductivity is related to a larger charge carrier concentration of 5×10^{21} holes/cm^3 vs 4×10^{21} holes/cm^3,[111] and the increase in the Seebeck coefficient then stems from a larger first derivate of the densities of states, c.f. eq 2.

Like in $Yb_{14}MnSb_{11}$, *ZT* increases sharply with increasing temperature, e.g. to 0.80 at 1050 K for $Mo_3Sb_{5.4}Te_{1.6}$ and to 0.93 at 1023 K for $Ni_{0.06}Mo_3Sb_{5.4}Te_{1.6}$. Thus far, varying t,he Te content from 1.5 to 1.7 yielded the highest *ZT* values at 1.6 Te per formula unit, and the only studies of quaternary $A_yMo_3Sb_{7-x}Te_x$ were performed on *A* = Fe and Ni, with the Ni samples exhibiting better thermoelectric performance. Other metal atoms *A* are under investigation, e.g., *A* = Mg, Mn, Co, Cu, as well as substitution on the Mo site as well as the Sb/Te sites. A completely different but isostructural set of materials is based on modification of Re_3As_7, e.g., by replacing As in part with Si, Ge, Sn.[108,112,113] These materials all show *n*-type conduction, a consequence of Re_3As_7 having 56 valence electrons per formula unit, compared to the 53 of Mo_3Sb_7. The *ZT* values determined thus far are slightly lower than those of their Mo_3Sb_7 counterparts, whereas studies of intercalations into the As cubes have just begun.

4. Summary

Recent results on new thermoelectric materials based on complex silicides, germanides, and antimonides were summarized in this review. All of the materials presented achieve ZT values around unity at elevated temperatures, and are thus of interest for power generation. At least both the filled skutterudites and $Yb_{14}MnSb_{11}$ are being investigated for power generation in automobiles and spacecrafts by the automobile industry and NASA, respectively.

The clathrates, formed mostly by silicides and germanides, are typical PGEC materials, e.g., with Ba atoms rattling in their dodecahedral and tetrakaidecahedral cages, while the antimony-based filled skutterudites were long thought to be PGEC materials as well. However, a recent investigation casted some doubt onto this, although the filler atoms do exhibit enlarged thermal parameters in their icosahedral cages. Two other antimonides, β-Zn_4Sb_3 and $Yb_{14}MnSb_{11}$, exhibit even lower thermal conductivity than the filled skutterudites, caused by positional Zn atom disorders and enhanced vibration of the Sb atoms along the linear chain in β-Zn_4Sb_3 and a highly complex structure in case of $Yb_{14}MnSb_{11}$.

The $A_yMo_3Sb_{7-x}Te_x$ family exhibits the highest thermal conductivity values of the materials presented here, and might therefore benefit the most from nanostructuring in the near future. Finally, it is evident that none of these investigations are finalized, i.e., the materials discussed here continue to be optimized. Considering for example that the ZT of doped PbTe more than doubled after nanostructuring, as reported for the quaternary PbTe-variant $AgPb_{18}SbTe_{20}$,[15] or band structure engineering, as reported for $Tl_{0.02}Pb_{0.98}Te$,[114] ZT values >2 are not unrealistic for such nanostructured or engineered bulk materials based on silicides, germanides, and antimonides.

Acknowledgment. Financial support from NSERC and the Canada Research Chair program is appreciated. Acknowledgment is made to the Donors of the American Chemical Society Petroleum Research Fund for partial support of this research.

References

(1) Tritt, T. M. *Science* **1999**, *283*, 804–805.
(2) DiSalvo, F. J. *Science* **1999**, *285*, 703–706.
(3) Bell, L. E. *Science* **2008**, *321*, 1457–1461.
(4) http://www1.eere.energy.gov/vehiclesandfuels/technologies/engines/waste_heat.html.
(5) Yang, J.; Caillat, T. *Mater. Res. Bull.* **2006**, *31*, 224–229.
(6) Tritt, T.; Böttner, H.; Chen, L. *Mater. Res. Bull.* **2008**, *33*, 366–368.
(7) Rowe, D. M., *Thermoelectrics Handbook: Macro to Nano*; CRC Press, Taylor & Francis Group: Boca Raton, FL, 2006.
(8) Snyder, G. J.; Toberer, E. S. *Nat. Mater.* **2008**, *7*, 105–114.
(9) Sofo, J. O.; Mahan, G. D. *Phys. Rev. B* **1994**, *49*, 4565–4570.
(10) Mott, N. F.; Jones, H., *The Theory of the Properties of Metals and Alloys*; Dover Publications: New York, 1958; p 310.
(11) Mahan, G. D.; Sofo, J. O. *Proc. Natl. Acad. Sci. U.S.A.* **1996**, *93*, 7436–7439.
(12) Rao, A.; Ji, X.; Tritt, T. M. *Mater. Res. Bull.* **2006**, *31*, 218–223.
(13) Franz, R.; Wiedemann, G. *Ann. Phys.* **1853**, *165*, 497–531.
(14) Lorenz, L. *Ann. Phys. Chem.* **1872**, *223*, 429–452.
(15) Hsu, K. F.; Loo, S.; Guo, F.; Chen, W.; Dyck, J. S.; Uher, C.; Hogan, T.; Polychroniadis, E. K.; Kanatzidis, M. G. *Science* **2004**, *303*, 818–821.
(16) Sootsman, J. R.; Kong, H.; Uher, C.; D'Angelo, J. J.; Wu, C.-I.; Hogan, T. P.; Caillat, T.; Kanatzidis, M. G. *Angew. Chem., Int. Ed.* **2008**, *47*, 8618–8622.
(17) Faleev, S. V.; Léonard, F. *Phys. Rev. B* **2008**, *77*, 214304/1–214304/9.
(18) Slack, G. A. New Materials and Performance Limits for Thermoelectric Cooling. In *CRC Handbook of Thermoelectrics*; Rowe, D. M., Ed.; CRC Press: Boca Raton, FL, 1995; pp 407−440.
(19) Slack, G. A. *Mater. Res. Soc. Symp. Proc.* **1997**, *478*, 47–54.
(20) Nolas, G. S.; Slack, G. A.; Schujman, S. B. *Semicond. Semimet.* **2001**, *69*, 255–300.
(21) Nolas, G. S.; Morelli, D. T.; Tritt, T. M. *Annu. Rev. Mat. Sci.* **1999**, *29*, 89–116.
(22) Kauzlarich, S. M.; Brown, S. R.; Snyder, G. J. *Dalton Trans.* **2007**, 2099–2107.
(23) Terasaki, I.; Sasago, Y.; Uchinokura, K. *Phys. Rev. B* **1997**, *56*, R12685–R12687.
(24) Terasaki, I. *Physica B* **2003**, *328*, 63–67.
(25) Poudeu, P. F. P.; D'Angelo, J.; Downey, A. D.; Short, J. L.; Hogan, T. P.; Kanatzidis, M. G. *Angew. Chem., Int. Ed.* **2006**, *45*, 3835–3839.
(26) Wölfing, B.; Kloc, C.; Teubner, J.; Bucher, E. *Phys. Rev. Lett.* **2001**, *86*, 4350–4353.
(27) May, A. F.; Fleurial, J.-P.; Snyder, G. J. *Phys. Rev. B* **2008**, *78*, 125205/1–125205/12.
(28) Poon, S. J. *Semicond. Semimet.* **2001**, *70*, 37–75.
(29) Shutoh, N.; Sakurada, S. *J. Alloys Compd.* **2005**, *389*, 204–208.
(30) von Stackelberg, M. *Naturwissenschaften* **1949**, *36*, 327–333.
(31) von Stackelberg, M. *Naturwissenschaften* **1949**, *36*, 359–362.
(32) Iversen, B. B.; Palmqvist, A. E. C.; Cox, D. E.; Nolas, G. S.; Stucky, G. D.; Blake, N. P.; Metiu, H. *J. Solid State Chem.* **2000**, *149*, 455–458.
(33) Bobev, S.; Sevov, S. C. *J. Am. Chem. Soc.* **1999**, *121*, 3795–3796.
(34) Guloy, A. M.; Ramlau, R.; Tang, Z.; Schnelle, W.; Baitinger, M.; Grin, Y. *Nature* **2006**, *443*, 320–323.
(35) Bobev, S.; Sevov, S. C. *J. Am. Chem. Soc.* **2001**, *123*, 3389–3390.
(36) Beekman, M.; Baitinger, M.; Borrmann, H.; Schnelle, W.; Meier, K.; Nolas, G. S.; Grin, Y. *J. Am. Chem. Soc.* **2009**, *131*, 9642–9643.
(37) Nesper, R. *Prog. Solid State Chem.* **1990**, *20*, 1–45.
(38) Zhao, J.-T.; Corbett, J. D. *Inorg. Chem.* **1994**, *33*, 5721–5726.
(39) Blake, N. P.; Mollnitz, L.; Kresse, G.; Metiu, H. *J. Chem. Phys.* **1999**, *111*, 3133–3144.
(40) Blake, N. P.; Bryan, D.; Latturner, S.; Møllnitz, L.; Stucky, G. D.; Metiu, H. *J. Chem. Phys.* **2001**, *114*, 10063–10074.
(41) Bentien, A.; Nishibori, E.; Paschen, S.; Iversen, B. B. *Phys. Rev. B* **2005**, *71*, 144107/1–144107/18.
(42) Chakoumakos, B. C.; Sales, B. C.; Mandrus, D. G.; Nolas, G. S. *J. Alloys Compd.* **2000**, *146*, 80–86.
(43) Bentien, A.; Palmqvist, A. E. C.; Bryan, J. D.; Latturner, S.; Stucky, G. D.; Furenlid, L.; Iversen, B. B. *Angew. Chem., Int. Ed.* **2000**, *39*, 3613–3616.
(44) Christensen, M.; Abrahamsen, A. B.; Christensen, N. B.; Juranyi, F.; Andersen, N. H.; Lefmann, K.; Andreasson, J.; Bahl, C. R. H.; Iversen, B. B. *Nat. Mater.* **2008**, *7*, 811–815.
(45) Blake, N. P.; Latturner, S.; Bryan, J. D.; Stucky, G. D.; Metiu, H. *J. Chem. Phys.* **2001**, *115*, 8060–8073.
(46) Uemura, T.; Akai, K.; Koga, K.; Tanaka, T.; Kurisu, H.; Yamamoto, S.; Kishimoto, K.; Koyanagi, T.; Matsuura, M. *J. Appl. Phys.* **2008**, *104*, 013702/1–013702/8.
(47) Tang, X.; Li, P.; Deng, S.; Zhang, Q. *J. Appl. Phys.* **2008**, *104*, 013706/1–013706/6.
(48) Pacheco, V.; Carrillo-Cabrera, W.; Tran, V. H.; Paschen, S.; Grin, Y. *Phys. Rev. Lett.* **2001**, *87*, 099602.
(49) Paschen, S.; Gspan, C.; Grogger, W.; Dienstleder, M.; Laumann, S.; Pongratz, P.; Sassik, H.; Wernisch, J.; Prokofiev, A. *J. Cryst. Growth* **2008**, *310*, 1853–1858.
(50) Saramat, A.; Svensson, G.; Palmqvist, A. E. C.; Stiewe, C.; Mueller, E.; Platzek, D.; Williams, S. G. K.; Rowe, D. M.; Bryan, J. D.; Stucky, G. D. *J. Appl. Phys.* **2006**, *99*, 023708/1–023708/5.
(51) Cao, W.-Q.; Yan, Y.-G.; Tang, X.-F.; Deng, S.-K. *J. Phys. D* **2008**, *41*, 215105/1–215105/6.
(52) Kuznetsov, V. L.; Kuznetsova, L. A.; Kaliazin, A. E.; Rowe, D. M. *J. Appl. Phys.* **2000**, *87*, 7871–7875.
(53) Deng, S.; Tang, X.; Li, P.; Zhang, Q. *J. Appl. Phys.* **2008**, *103*, 073503/1–073503/6.
(54) Caillat, T.; F., J. P.; Borshchevsky, A. *J. Phys. Chem. Solids* **1997**, *58*, 1119–1125.
(55) Brown, S. R.; Kauzlarich, S. M.; Gascoin, F.; Snyder, G. J. *Chem. Mater.* **2006**, *18*, 1873–1877.
(56) Dashjav, E.; Szczepenowska, A.; Kleinke, H. *J. Mater. Chem.* **2002**, *12*, 345–349.
(57) Gascoin, F.; Rasmussen, J.; Snyder, G. J. *J. Alloys Compd.* **2007**, *427*, 324–329.
(58) Holgate, T.; Su, Z.; He, J.; Tritt, T. M.; Xu, H.; Kleinke, K. M.; Kleinke, H. *MS&T'08 Conference Proceedings*; Pittsburgh, PA, Oct 5−9, 2008; MS&T Partner Societies, 2008; pp 436−443
(59) Xu, H.; Kleinke, K. M.; Holgate, T.; Zhang, H.; Su, Z.; Tritt, T. M.; Kleinke, H. *J. Appl. Phys.* **2009**, *105*, 053703/1–053703/5.
(60) Gascoin, F.; Ottensmann, S.; Stark, D.; Haïle, S. M.; Snyder, G. J. *Adv. Funct. Mater.* **2005**, *15*, 1860–1864.

(61) Yu, C.; Zhu, T. J.; Zhang, S. N.; Zhao, X. B.; He, J.; Su, Z.; Tritt, T. M. *J. Appl. Phys.* **2008**, *104*, 013705/1–013705/5.
(62) Wang, X.-J.; Tang, M.-B.; Chen, H.-H.; Yang, X.-X.; Zhao, J.-T.; Burkhardt, U.; Grin, Y. *Appl. Phys. Lett.* **2009**, *94*, 092106/1–092106/3.
(63) Braun, D. J.; Jeitschko, W. *J. Less-Common Met.* **1980**, *72*, 147–156.
(64) Chakoumakos, B. C.; Sales, B. C.; Mandrus, D.; Keppens, V. *Acta Crystallogr., Sect. B* **1999**, *55*, 341–347.
(65) Zhao, W. Y.; Dong, C. L.; Wei, P.; Guan, W.; Liu, L. S.; Zhai, P. C.; Tang, X. F.; Zhang, Q. J. *J. Appl. Phys.* **2007**, *102*, 113708/1–113708/6.
(66) Uher, C. *Semicond. Semimet.* **2001**, *69*, 139–253.
(67) Koza, M. M.; Johnson, M. R.; Viennois, R.; Mutka, H.; Girard, L.; Ravot, D. *Nat. Mater.* **2008**, *7*, 805–810.
(68) Kjekshus, A.; Rakke, T. *Acta Chem. Scand.* **1974**, *28*, 99–103.
(69) Hönle, W.; von Schnering, H.-G. *Z. Kristallogr.* **1981**, *155*, 307–314.
(70) Korber, N.; Richter, F. *Angew. Chem., Int. Ed.* **1997**, *36*, 1512–1514.
(71) Kleinke, H. *Chem. Commun.* **2000**, 1941–1942.
(72) Sales, B. C.; Mandrus, D.; Williams, R. K. *Science* **1996**, *272*, 1325–1328.
(73) Fornari, M.; Singh, D. J. *Appl. Phys. Lett.* **1999**, *74*, 3666–3668.
(74) Fornari, M.; Singh, D. J. *Phys. Rev. B* **1999**, *59*, 9722–9724.
(75) Anno, H.; Ashida, K.; Matsubara, K.; Nolas, G. S.; Akai, K.; Matsuura, M.; Nagao, J. *Mater. Res. Soc. Symp. Proc.* **2002**, *691*, 49–54.
(76) Xu, J.; Kleinke, H. *J. Comput. Chem.* **2008**, *29*, 2134–2143.
(77) Nolas, G. S.; Kaeser, M.; Littleton, R. T. I.; Tritt, T. M. *Appl. Phys. Lett.* **2000**, *77*, 1855–1857.
(78) Puyet, M.; Dauscher, A.; Lenoir, B.; Dehmas, M.; Stiewe, C.; Müller, E. *J. Appl. Phys.* **2005**, *97*, 083712/1–083712/4.
(79) Chen, L. D.; Kawahara, T.; Tang, X. F.; Goto, T.; Hirai, T.; Dyck, J. S.; Chen, W.; Uher, C. *J. Appl. Phys.* **2001**, *90*, 1864–1868.
(80) Chitroub, M.; Besse, F.; Scherrer, H. *J. Alloys Compd.* **2008**, *460*, 90–93.
(81) Snyder, G. J.; Christensen, M.; Nishibori, E.; Caillat, T.; Iversen, B. B. *Nat. Mater.* **2004**, *3*, 458–463.
(82) Mozharivskyj, Y.; Janssen, Y.; Harringa, J. L.; Kracher, A.; Tsokol, A. O.; Miller, G. J. *Chem. Mater.* **2006**, *18*, 822–831.
(83) Nylén, J.; Lidin, S.; Andersson, M.; Iversen, B. B.; Liu, H.; Newman, N.; Häussermann, U. *Chem. Mater.* **2007**, *19*, 834–838.
(84) Kim, S.-G.; Mazin, I. I.; Singh, D. J. *Phys. Rev. B* **1998**, *57*, 6199–6203.
(85) Kim, H. J.; Božin, E. S.; Haile, S. M.; Snyder, G. J.; Billinge, S. J. L. *Phys. Rev. B* **2007**, *75*, 134103/1–134103/4.
(86) Schweika, W.; Hermann, R. P.; Prager, M.; Persson, J.; Keppens, V., Phys. Rev. Lett. **2007**, 2007, 125501/1-125501/4.
(87) Li, D.; Hng, H. H.; Ma, J.; Qin, X. Y. *J. Mater. Res.* **2008**, *24*, 430–435.
(88) Pedersen, B. L.; Birkedal, H.; Nygren, M.; Frederiksen, P. T.; Iversen, B. B. *J. Appl. Phys.* **2009**, 105.
(89) Ueno, K.; Yamamoto, A.; Noguchi, T.; Inoue, T.; Sodeoka, S.; Obara, H. *J. Alloys Compd.* **2005**, *388*, 118–121.
(90) Cordier, G.; Schäfer, H.; Stelter, M. *Z. Anorg. Allg. Chem.* **1984**, *519*, 183–188.
(91) Tasman, H. A.; Boswijk, K. H. *Acta Crystallogr.* **1955**, *8*, 59–60.
(92) Mooney Slater, R. C. L. *Acta Crystallogr.* **1959**, *12*, 187–196.
(93) Assoud, A.; Xu, J.; Kleinke, H. *Inorg. Chem.* **2007**, *46*, 9906–9911.
(94) Gallup, R. F.; Fong, C. Y.; Kauzlarich, S. M. *Inorg. Chem.* **1992**, *31*, 115–118.
(95) Hermann, R. P.; Grandjean, F.; Kafle, D.; Brown, D. E.; Johnson, C. E.; Kauzlarich, S. M.; Long, G. J. *Inorg. Chem.* **2007**, *46*, 10736–10740.
(96) Sánchez-Portal, D.; Martin, R. M.; Kauzlarich, S. M.; Pickett, W. E. *Phys. Rev. B* **2002**, *65*, 144414/1–144414/15.
(97) Carrillo-Cabrera, W.; Somer, M.; Peters, K.; von Schnering, H. G. *Chem. Ber.* **1996**, *129*, 1015–1023.
(98) Young, D. M.; Torardi, C. C.; Olmstead, M. M.; Kauzlarich, S. M. *Chem. Mater.* **1995**, *7*, 93–101.
(99) Rehr, A.; Kuromoto, T. Y.; Kauzlarich, S. M.; Del Castillo, J.; Webb, D. J. *Chem. Mater.* **1994**, *6*, 93–99.
(100) Kauzlarich, S. M.; Thomas, M. M.; Odink, D. A.; Olmstead, M. M. *J. Am. Chem. Soc.* **1991**, *113*, 7205–7208.
(101) Chan, J. Y.; Olmstead, M. M.; Kauzlarich, S. M.; Webb, D. J. *Chem. Mater.* **1998**, *10*, 3583–3588.
(102) Toberer, E. S.; Brown, S. R.; Ikeda, T.; Kauzlarich, S. M.; Snyder, G. J. *Appl. Phys. Lett.* **2008**, *93*, 062110/1–062110/3.
(103) Brown, S. R.; Toberer, E. S.; Ikeda, T.; Cox, C. A.; Gascoin, F.; Kauzlarich, S. M.; Snyder, G. J. *Chem. Mater.* **2008**, *20*, 3412–3419.
(104) Toberer, E. S.; Cox, C. A.; Brown, S. R.; Ikeda, T.; May, A. F.; Kauzlarich, S. M.; Snyder, G. J. *Adv. Funct. Mater.* **2008**, *18*, 2795–2800.
(105) Cox, C. A.; Toberer, E. S.; Levchenko, A. A.; Brown, S. R.; Snyder, G. J.; Navrotsky, A.; Kauzlarich, S. M. *Chem. Mater.* **2009**, *21*, 1354–1360.
(106) Brown, A. *Nature* **1965**, *206*, 502–503.
(107) Soheilnia, N.; Dashjav, E.; Kleinke, H. *Can. J. Chem.* **2003**, *81*, 1157–1163.
(108) Soheilnia, N.; Xu, H.; Zhang, H.; Tritt, T. M.; Swainson, I.; Kleinke, H. *Chem. Mater.* **2007**, *19*, 4063–4068.
(109) Candolfi, C.; Lenoir, B.; Dauscher, A.; Tobola, J.; Clarke, S. J.; Smith, R. I. *Chem. Mater.* **2008**, *20*, 6556–6561.
(110) Candolfi, C.; Lenoir, B.; Dauscher, A.; Guilmeau, E.; Hejtmanek, J.; Tobola, J.; Wiendlocha, B.; Kaprzyk, S. *Phys. Rev. B* **2009**, *79*, 035114/1–035114/6.
(111) Zhang, H.; He, J.; Zhang, B.; Su, Z.; Tritt, T. M.; Soheilnia, N.; Kleinke, H. *J. Electron. Mater.* **2007**, *36*, 727–731.
(112) Xu, H.; Soheilnia, N.; Zhang, H.; Alboni, P. N.; Tritt, T. M.; Kleinke, H. *Mater. Res. Soc. Symp. Proc.* **2008**, *1044*, 459–467.
(113) Xu, H.; Holgate, T.; He, J.; Su, Z.; Tritt, T. M.; Kleinke, H. *J. Electron. Mater.* **2009**, *38*, 1030–1036.
(114) Heremans, J. P.; Jovovic, V.; Toberer, E. S.; Saramat, A.; Kurosaki, K.; Charoenphakdee, A.; Yamanaka, S.; Snyder, G. J. *Science* **2008**, *321*, 554–557.